

THz near-field enhancement by means of isolated dipolar antennas: the effect of finite sample size

Matteo Savoini,^{1,2,*} Sebastian Grübel,^{1,2} Salvatore Bagiante,^{3,4} Hans Sigg,³ Thomas Feurer,⁴ Paul Beaud,^{2,5} and Steven L. Johnson^{1,2}

¹*Institute for Quantum Electronics, Eidgenössische Technische Hochschule (ETH) Zürich, Auguste-Piccard-Hof 1, 8093 Zürich, Switzerland*

²*Swiss Light Source, Paul Scherrer Institute, 5232 Villigen PSI, Switzerland*

³*Laboratory of Micro- and Nanotechnology, Paul Scherrer Institute, Villigen 5232, Switzerland*

⁴*Institute of Applied Physics, University of Bern, Bern 3012, Sidlerstrasse 5, Switzerland*

⁵*SwissFEL, Paul Scherrer Institut, CH-5232 Villigen PSI, Switzerland*

[*savoinim@phys.ethz.ch](mailto:savoinim@phys.ethz.ch)

Abstract: Generation of high intensity terahertz radiation in the low frequency region ($f < 5$ THz) is still a challenging task and only few experimental demonstrations exceeding 1 MV/cm have been reported so far. One viable option is the use of resonant metallic structures which act as amplifiers for the impinging radiation. Here with the aid of finite difference time domain simulations, we design and realize a set of isolated resonant elements which allow us to reach a 28-fold enhancement of freely propagating THz radiation at $f \approx 1$ THz. These elements are deposited on a GaP sample allowing the direct measurement of the field enhancement using electro-optical sampling. Interestingly, we experimentally show strong modifications of the antennas resonance which is interpreted in terms of interference effects. These are particularly important in samples thinner than half the spatial pulse length.

© 2016 Optical Society of America

OCIS codes: (040.2235) Far infrared or terahertz; (050.6624) Subwavelength structures; (160.2100) Electro-optical materials; (160.4890) Organic materials; (190.7110) Ultrafast nonlinear optics; (320.5390) Picosecond phenomena; (320.7150) Ultrafast spectroscopy.

References and links

1. M. C. Hoffmann and J. A. Fülöp, "Intense ultrashort terahertz pulses: generation and applications," *J. Phys. (Paris) D: Appl. Phys.* **44**, 083001 (2011).
2. A. Schneider, M. Neis, M. Stillhart, B. Ruiz, R. U. A. Khan, and P. Günter, "Generation of terahertz pulses through optical rectification in organic DAST crystals: theory and experiment," *J. Opt. Soc. Am. B* **23**, 1822–1835 (2006).
3. C. P. Hauri, C. Ruchert, C. Vicario, and F. Ardana, "Strong-field single-cycle THz pulses generated in an organic crystal," *Appl. Phys. Lett.* **99**, 161116 (2011).
4. C. Ruchert, C. Vicario, C. P. Hauri, "Scaling submillimeter single-cycle transients toward megavolts per centimeter field strength via optical rectification in the organic crystal OH1," *Opt. Lett.* **37**, 899–901 (2012).
5. M. Liu, H. Y. Hwang, H. Tao, A. C. Strikwerda, K. Fan, G. R. Keiser, A. J. Sternbach, K. G. West, S. Kittiwatanakul, J. Lu, S. A. Wolf, F. G. Omenetto, X. Zhang, K. A. Nelson, and R. D. Averitt, "Terahertz-field-induced insulator-to-metal transition in vanadium dioxide metamaterial," *Nature (London)* **487**, 345–348 (2012).
6. T. Kubacka, J. A. Johnson, M. C. Hoffmann, C. Vicario, S. de Jong, P. Beaud, S. Grübel, S.-W. Huang, L. Huber, L. Patthey, Y.-D. Chuang, J. J. Turner, G. L. Dakovski, W.-S. Lee, M. P. Minitti, W. Schlotter, R. G. Moore, C.

- P. Hauri, S. M. Koohpayeh, V. Scagnoli, G. Ingold, S. L. Johnson, U. Staub, "Large-amplitude spin dynamics driven by a THz pulse in resonance with an electromagnon," *Science* **343**, 1333–1336 (2014).
7. T. Kampfrath, A. Sell, G. Klatt, A. Pashkin, S. Mährlein, T. Dekorsy, M. Wolf, M. Fiebig, A. Leitenstorfer, and R. Huber, "Coherent terahertz control of antiferromagnetic spin waves," *Nature (London) Photon.* **5**, 31–34 (2011).
 8. A. Dienst, M. C. Hoffmann, D. Fausti, J. C. Petersen, S. Pyon, T. Takayama, H. Takagi and A. Cavalleri, "Bidirectional ultrafast electric-field gating of interlayer charge transport in a cuprate superconductor," *Nat. Photon.* **5**, 485–488 (2011).
 9. A. H. M. Reid, Th. Rasing, R. V. Pisarev, H. A. Dürr and M. C. Hoffmann, "Terahertz-driven magnetism dynamics in the orthoferrite DyFeO₃," *Appl. Phys. Lett.* **106**, 082403 (2015).
 10. S. Grübel, J. A. Johnson, J. Rittmann, S. O. Mariager, P. Beaud, G. Ingold, A. Ferrer, T. Huber, L. Huber, T. Kubacka, S. L. Johnson, A. Kohutych, V. Haborets, and Y. Vysochanskii, "Ultrafast x-ray diffraction of a ferroelectric soft mode driven by broadband terahertz pulses," manuscript submitted.
 11. T. Huber, M. Ranke, A. Ferrer, L. Huber and S. L. Johnson, "Coherent phonon spectroscopy of non-fully symmetric modes using resonant terahertz excitation," *Appl. Phys. Lett.* **107**, 091107 (2015).
 12. R. Singh, I. A. I. Al-Naib, M. Koch, and W. Zhang, "Sharp Fano resonances in THz metamaterials," *Opt. Express* **19**, 6312–6319 (2011).
 13. F. Ma, Y.-S. Lin, X. Zhang and C. Lee, "Tunable multiband terahertz metamaterials using a reconfigurable electric split-ring resonator array," *Light Sci. Appl.* **3**, e171 (2014).
 14. K. Iwaszczuk, A. Andryeuskii, A. Lavrinenko, X.-C. Zhang, and P. U. Jepsen, "Terahertz field enhancement to the MV/cm regime in a tapered parallel plate waveguide," *Opt. Express* **20**, 8344–8355 (2012).
 15. A. J. L. Adam, "Review of near-field terahertz measurement methods and their applications: how to achieve sub-wavelength resolution at THz frequencies," *J. Infrared Milli. Terahz. Waves*, **32**, 976–1019 (2011).
 16. M. C. Schaafsma, H. Starmans, A. Berrier, and J. Gómez Rivas, "Enhanced terahertz extinction of single plasmonic antennas with conically tapered waveguides," *New J. Phys.* **15**, 015006 (2013).
 17. M. Shalaby, and C. P. Hauri, "Demonstration of a low-frequency three-dimensional terahertz bullet with extreme brightness," *Nature (London) Commun.* **6**, 5976 (2014).
 18. H. Merbold, A. Bitzer, and T. Feurer, "Second harmonic generation based on strong field enhancement in nanostructured THz materials," *Opt. Express* **19**, 7262–7273 (2011).
 19. S. Bagiante, F. Enderli, J. Fabiańska, H. Sigg, and T. Feurer, "Giant electric field enhancement in split ring resonators featuring nanometer-sized gaps," *Sci. Rep.* **5**, 8051 (2015).
 20. F. Enderli and T. Feurer, "Coherent control of terahertz meta-materials," *Appl. Phys. Lett.* **103**, 061903 (2013).
 21. M. A. Seo, H. R. Park, S. M. Koo, D. J. Park, J. H. Kang, O. K. Suwal, S. S. Choi, P. C. M. Planken, G. S. Park, N. K. Park, Q. H. Park and D. S. Kim, "Terahertz field enhancement by a metallic nano slit operating beyond the skin-depth limit," *Nature (London) Photon.* **3**, 152–156 (2009).
 22. H. R. Park, Y. M. Park, H. S. Kim, J. S. Kyoung, M. A. Seo, D. J. Park, Y. H. Ahn, K. J. Ahn, and D. S. Kim, "Terahertz nanoresonators: giant field enhancement and ultrabroadband performance," *Appl. Phys. Lett.* **96**, 121106 (2010).
 23. A. R. Davoyan, V. V. Popov, and S. A. Nikitov, "Tailoring terahertz near-field enhancement via two-dimensional plasmons," *Phys. Rev. Lett.* **108**, 127401 (2012).
 24. M. Shalaby, J. Fabiańska, M. Peccianti, Y. Ozturk, F. Vidal, H. Sigg, R. Morandotti, and T. Feurer, "Skirting terahertz waves in a photo-excited nanoslit structure," *Appl. Phys. Lett.* **104**, 171115 (2014).
 25. P. Mühlischlegel, H.-J. Eisler, O. J. F. Martin, B. Hecht, D. W. Pohl, "Resonant optical antennas," *Science* **308**, 1607–1609 (2005).
 26. H. Fischer and O. J. F. Martin, "Engineering the optical response of plasmonic nanoantennas," *Opt. Express* **16**, 9144–9154 (2008).
 27. C. A. Balanis, *Antenna Theory: Analysis and Design* (Wiley-Interscience, 1982).
 28. C. A. Werley, K. Fan, A. C. Strikwerda, S. M. Teo, X. Zhang, R. D. Averitt, and K. A. Nelson, "Time-resolved imaging of near-fields in THz antennas and direct quantitative measurement of field enhancements," *Opt. Express* **20**, 8551–8567 (2012).
 29. L. Razzari, A. Toma, M. Shalaby, M. Clerici, R. Proietti Zaccaria, C. Liberale, S. Marras, I. A. I. Al-Naib, G. Das, F. De Angelis, M. Peccianti, A. Falqui, T. Ozaki, R. Morandotti, and E. Di Fabrizio, "Extremely large extinction efficiency and field enhancement in terahertz resonant dipole nanoantennas," *Opt. Express* **19**, 26088–26094 (2011).
 30. V. Giannini, A. Berrier, S. A. Maier, J. A. Sánchez-Gil, and J. Gómez Rivas, "Scattering efficiency and near field enhancement of active semiconductor plasmonic antennas at terahertz frequencies," *Opt. Express* **18**, 2798–2807 (2010).
 31. B. Koene, M. Savoini, A. V. Kimel, A. Kirilyuk and Th. Rasing, "Optical energy optimization at the nanoscale by near-field interference," *Appl. Phys. Lett.* **101**, 013115 (2012).
 32. L. Novotny and B. Hecht, *Principles of Nano-Optics* (Cambridge University, 2006).
 33. Lumerical Solutions, Inc. <http://www.lumerical.com/tcad-products/fdtd/>
 34. E. D. Palik, *Handbook of Optical Constants of Solids* (Academic, 1998).
 35. M. A. Ordal, Robert J. Bell, R. W. Alexander, L. L. Long, and M. R. Querry, "Optical properties of fourteen

- metals in the infrared and far infrared: Al, Co, Cu, Au, Fe, Pb, Mo, Ni, Pd, Pt, Ag, Ti, V, and W,” *Appl. Opt.* **24**, 4493–4499 (1985).
36. J. H. Kang, D. S. Kim, and Q.-H. Park, “Local capacitor model for plasmonic electric field enhancement,” *Phys. Rev. Lett.* **102**, 093906 (2009).
 37. L. Novotny, “Effective wavelength scaling for optical antennas,” *Phys. Rev. Lett.* **98**, 266802 (2007).
 38. T. H. Taminiau, F. D. Stefani, F. B. Segerink, and N. F. van Hulst, “Optical antennas direct single-molecule emission,” *Nature (London) Photon.* **2**, 234–237 (2008).
 39. M. Born, and E. Wolf, *Principles of Optics: Electromagnetic Theory of Propagation, Interference and Diffraction of Light* (Pergamon, 1959).
 40. F. D. J. Brunner, J. A. Johnson, S. Gröbel, A. Ferrer, S. L. Johnson, and T. Feurer “Distortion-free enhancement of terahertz signals measured by electro-optic sampling. I. Theory,” *J. Opt. Soc. Am. B* **31**, 904–910 (2014).
 41. J. A. Johnson, F. D. J. Brunner, S. Gröbel, A. Ferrer, S. L. Johnson, and T. Feurer “Distortion-free enhancement of terahertz signals measured by electro-optic sampling. II. Experiment,” *J. Opt. Soc. Am. B* **31**, 1035–1040 (2014).
 42. A. R. Khorsand, M. Savoini, A. Kirilyuk, A. V. Kimel, A. Tsukamoto, A. Itoh, and Th. Rasing, “Role of magnetic circular dichroism in all-optical magnetic recording,” *Phys. Rev. Lett.* **108**, 127205 (2012).
 43. A. R. Khorsand, M. Savoini, A. Kirilyuk, and Th. Rasing, “Optical excitation of thin magnetic layers in multilayer structures,” *Nature (London) Mater.* **13**, 101–102 (2014).
-

1. Introduction

THz radiation has received increasing attention in the last decades, thanks in part to the availability of high efficiency optical rectification materials such as LiNbO₃, and/or the most common organic crystals, i.e. (2-(3-(4-Hydroxystyryl)-5,5-dimethylcyclohex-2-enylidene)malononitrile) [OH1], 4-N,N-dimethylamino-4'-N'-methyl-stilbazolium 2,4,6-trimethylbenzenesulfonate [DSTMS], and 4-N,N-dimethylamino-4'-N'-methyl-stilbazolium tosylate [DAST] [1–4].

Although these improved THz sources have enabled first investigations of coherent control of various material properties using THz-radiation [5–11], they have also shown that in order to achieve a persistent switching of a ferroelectric or (anti)ferromagnetic orientations as desired for many potential applications, peak field strengths exceeding 5-15 MV/cm at frequencies of 1-2 THz are generally required [5, 6, 10]. One promising approach to achieve such high peak THz-fields as well as effective frequency tunability is the application of metamaterial metallic structures incorporated into the material that are specifically designed to enhance the incoming THz-field [5]. The primary drawback of this approach is the extremely complex machining of the surface, requiring a coverage of large areas with features smaller than 1 μm in size [5, 12, 13]. Moreover they rely on the excitation of localized carrier which resonate and amplify the impinging radiation. These structures are therefore most efficient for enhancing the incoming THz-radiation into insulating samples in the wavelength range under investigation.

Other approaches for high field enhancements involve the use of tapered metallic or even semiconducting plates, which can enhance fields for materials placed within the gap between the plates or in very close proximity. With this type of design, THz fields as high as 1-2 MV/cm have been reported [14–16]. Moreover a careful optimization of the focusing apparatus can also help; very recently extremely large peak electric fields exceeding 50 MV/cm have been reported for source parameters that normally would lead to only a few MV/cm fields [17]. Both methods achieve high field amplitude without complex machining of the sample surface for frequency $f < 5$ THz, but pose strong limitations on the sample geometry and/or rely on an extremely precise positioning of sample and optical elements which is not always practical, together with the use of extremely powerful lasers.

Still another approach is the use of the near-field (NF) enhancement of THz fields from isolated metallic elements deposited on the sample surface. This would allow for localized strong field enhancements, without the requirement to functionalize the entire sample surface. This enhancement method has been generally explored in only a few geometries, namely in

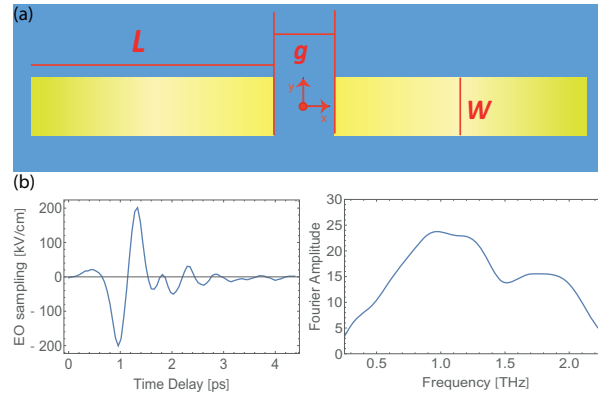


Fig. 1. (a) Sketch of the antenna geometry: L is the arm length, g the gap size, and W the antenna width. Gap center is the origin of the reference system. (b) Typical THz-radiation pulse shape in time domain [left] and its relative Fourier spectrum [right].

split-ring resonator [18–20], nano-slits [21–24] and dipolar antennas [25, 26, 28–31].

Here we present a relatively simple experimental setup able to directly measure the NF enhancement generated by Au-dipolar antennas deposited directly on an active thin layer of GaP. We focus our attention on dipolar antennas because they are (i) extremely easy to fabricate, being made up by two rods with a common feedgap, (ii) present strong field enhancements, easily tunable by changing the arm length, and (iii) are readily modeled in an approximate way using simple methods. Interestingly we measure strong modulations of the NF enhancement. With the aid of computer simulations, we are able to explain these in terms of interference effects of the propagating THz-field within a sample with a thickness comparable to the radiation wavelength. By taking advantage of these effects, we are able to achieve enhancements larger than 28 times, resulting in peak fields of more than 5 MV/cm at a frequency around 1 THz and at a repetition rate of 1 KHz for externally coupled THz pulses.

2. Antenna design and simulations

We consider Au antenna structures as depicted in Fig. 1(a), consisting of two aligned gold nanorods separated by a small gap. As the length of the two arms is increased, the antenna resonance is red-shifted, accordingly with the behavior of the resonances supported by nanorods when their aspect ratio is varied [32]. We have deposited these structures directly on a GaP sample, which is a standard dielectric material (roughly no absorption below 11 THz, thus $Im(n) \approx 0$) to measure the amplitude of the impinging THz radiation through Electro-Optic (EO) sampling. The THz radiation is generated by an OH1 organic crystal, as described in more detail in the following. A typical time trace and spectrum of the THz pulse is represented in Fig. 1(b).

To evaluate the effects of the antenna parameters on the THz field in the vicinity of the gap, we employed a commercial-grade simulator based on the finite-difference time-domain method to simulate the NF dynamics [33]. In particular we study a dipole Au antenna with volume of a single arm of $L \times 10 \times 0.1 \mu\text{m}^2$ and gap size of $4 \mu\text{m}$. A non-uniform three-dimensional discretization mesh of $0.5 \times 0.5 \times 0.01 \mu\text{m}^3$ is used. We consider a broadband plane-wave illumination at frequencies in the range 0.4–2.3 THz with a spectrum similar to the one of Fig. 1(b). The radiation is linearly polarized along x , with direction of incidence perpendicular to the sample surface. The GaP layer is modeled with a dielectric constant $\epsilon = 11.16$ [34], while the upper

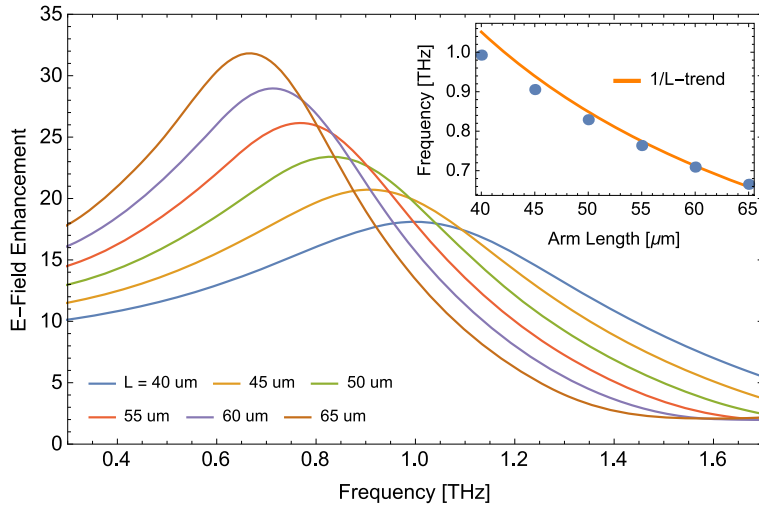


Fig. 2. Frequency-dependent field enhancement as a function of the antenna arm length L . Inset: Frequency position of the maximum enhancement, compared with a simple $1/L$ model (solid line).

half space is vacuum. The permittivity of gold in is approximated by a simple Drude model, gold being very close to a perfect metal in this frequency range [35].

We calculate the field amplitudes as a function of the antenna arm length L over a range from 40 to 65 μm , in steps of 5 μm . For each L , we determine the field in the center of the feed gap [position $(x, y, z) = (0, 0, 0.05) \mu\text{m}$, medium = air] and calculate its relative frequency-dependent amplitude with respect to the field simulated in the absence of the antenna. The results are displayed in Fig. 2. Two features are clearly apparent: with increasing antenna length the resonance peak frequency shifts towards lower frequencies and the resonance amplitude increases. Both aspects can be readily explained by a simple model. The common feed gap can be considered as a capacitive element [36], which determines the coupling strength between the two antenna arms. As a matter of fact, the resonance wavelength of a long antenna is larger than that of a short antenna. Hence, there is an increase in the interaction cross-section with the impinging radiation. Moreover the gap has a smaller effective length for the larger antenna, which results in a stronger coupling between both arms, leading to a linear increase in the field enhancement with the antenna length [26].

Regarding the shift in frequency, microwave theory predicts that antennas in free space will have a maximum efficiency when the arm length is an odd-integer multiple m of half wavelengths [27–30]: therefore we expect a simple $1/L$ -model could reasonably fit the resonance frequency position f_{res} . In the THz frequency range no corrections are needed to account for non-ideal behavior of metallic surfaces, as required in the visible range [37]. Moreover, in case of high-index surfaces, such as GaP, the antenna response can be considered to be dependent solely on the higher index material, as if it would completely be embedded in the sample [28, 29]. The Inset of Fig. 2 shows the peak positions (points) in good agreement with the $1/L$ -model (solid line), computed using the tabulated value $n = 3.34$ for GaP [1, 34].

It is worth noting that if the linear polarization of the illuminating beam is not parallel to the antenna axis, only the field projection along the main axis will be enhanced [38]. This argument is valid as long the antenna aspect ratio (length/width) is large enough to have a clear separation between the resonances parallel and perpendicular to the main axis.

In this section we have evaluated the antenna behavior in the assumption of a semi-infinite substrate. Simulated field enhancements in the antenna plane can be as high as a factor of 30 even in the presence of relatively large antenna gaps (4 μm in this case). Larger field amplitudes could be obtained tuning the antenna length to resonate at lower frequencies and/or by decreasing the gap size [28, 36]. As discussed above, the presence and optical properties of the substrate strongly influence the antenna resonance behavior even more in the case of a finite substrate thickness, which will be discussed in the next section.

3. Finite sample thickness

The frequency range 0.1-10 THz is characterized by a free space wavelength in the range 30 to 3000 μm . If these dimensions are comparable to or less than the thickness of the substrate, the antenna response can be dramatically modified.

As an example we consider a 100- μm thick slab of GaP. The finite thickness of the slab will produce two sets of reflected and transmitted beams at both interfaces. Depending on the exact optical path length, these reflections can interfere destructively or constructively. The overall reflection of a layer structure is thus the sum of an infinite number of reflections, and can be computed for example via the transfer-matrix method [39].

The transfer-matrix element for a thin slab of non-absorbing material is:

$$M = \begin{pmatrix} \cos(k'd) & \sin(k'd)/k' \\ -k' \sin(k'd) & \cos(k'd) \end{pmatrix}, \quad (1)$$

where $k' = nk$, with $k = 2\pi/\lambda$ being the radiation wavenumber in free-space at normal incidence on the slab, λ the free-space wavelength, n and d the slab refractive index and thickness. From the matrix element we can calculate the field reflection coefficient r :

$$r = \frac{(1/n - n) \sin(k'd)}{(n + 1/n) \sin(k'd) + 2i \cos(k'd)}. \quad (2)$$

The intensity reflection coefficient $R = rr^*$ is effectively zero for $k'd = 0, \pi, 2\pi, \dots$, which translates for $n = 3.34$ and $d = 100 \mu\text{m}$ to nodes in the reflectivity at the frequencies $f_{R=0} \approx m \cdot 0.469 \text{ THz}$, with $m = 1, 2, 3, \dots$. Thus for all $f_{R=0}$ nodes, the impinging THz radiation is transmitted unaltered into the GaP slab. In between these nodes we find a high reflectivity point ($R \approx 70\%$), strongly limiting the transmitted amount of radiation. The modulation of the incoming THz pulse is presented in Fig. 3(a) [Dashed red line]. The modulation of the impinging radiation has indeed an enormous effect also on the antenna enhancement, as presented in Fig. 3(a). Rather than observing a single Lorentzian shape, as shown in Fig. 2, a three-lobed field distribution is simulated. The relative amplitude of these three maxima changes significantly with antenna length. For example for the $L = 40 \mu\text{m}$ case, we observe a rather symmetric distribution with a larger central peak; on the other hand, the electric field amplitude in the 65 μm -antenna gap shows a clear predominance of the low frequency components. Notably, even the peak frequencies present a different behavior for the different lobes as a function of the antenna length. The low- and high-frequency maxima, in fact, do not significantly shift with L , while the central peak amplitude does. This is easily explained by the design of the antennas under investigation: at the simulated lengths the resonance peak travel through the frequency selected by the central modulation (see Fig. 2), only changing the amplitude of the maximum enhancement in the two other frequency ranges.

Figure 3(b) shows the calculated enhancement in the spectral range, obtained by dividing the E-field amplitude curves [Solid lines in Fig. 3(a)] by the reference with no antenna present [Dashed red line]. It is apparent how the frequency modulation induced by the etalon effect from the finite GaP thickness produces a significant distortion in the antenna enhancement

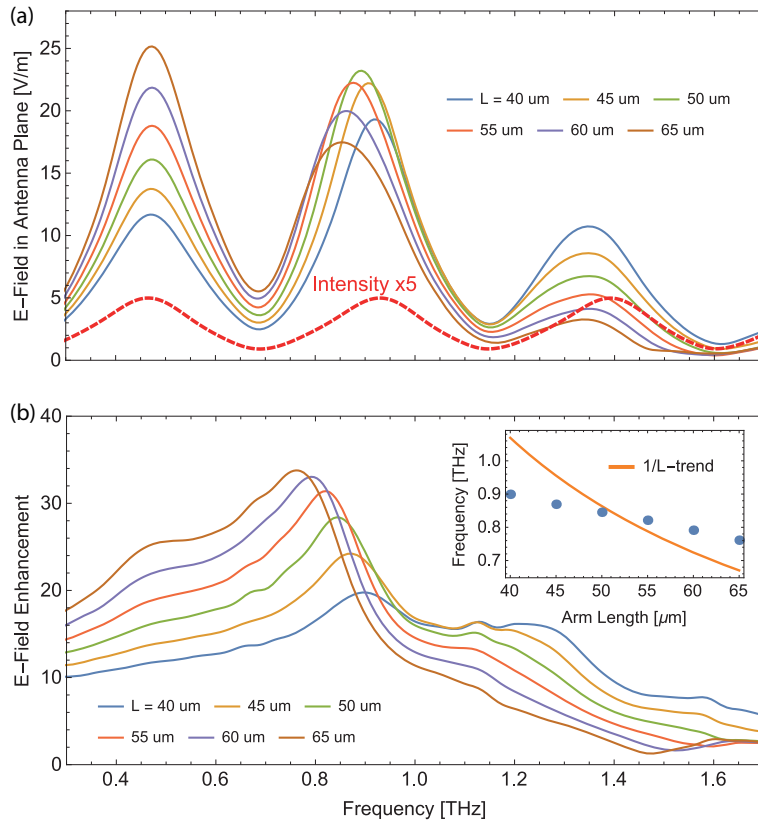


Fig. 3. (a) Frequency-dependent field amplitude as a function of the antenna arm length L in the case of a finite substrate thickness. Red dashed line: Electric-field amplitude modulation ($\times 5$) for a perpendicular THz pulse impinging on a bare GaP slab (in absence of antenna structures). (b) Frequency-dependent field amplitude as a function of the antenna arm length L . Inset: Frequency position of the maximum enhancement, compared with the model used in Fig. 2.

factor. In particular, the maximum enhancement frequency-position strongly deviates from the one computed with the simple half-wave antenna model for a semi-infinite substrate [Inset of Fig. 3(b)].

This last point implies that the finite thickness of the sample should be taken into account for a precise design of the antenna geometry, because it could significantly shift the expected resonance peak position. In particular, by a clever matching of resonance frequency and the modulation one, a much larger enhancement can be achieved in thin samples compared to semi-infinite ones. This holds particularly true for any thin samples with a complex refractive index \tilde{n} when the following conditions are satisfied: $\text{Re}[\tilde{n}] \cdot d \approx \lambda$ and $\alpha \cdot d \ll 1/\text{Re}[\tilde{n}]$, where $\alpha = 2\pi/\lambda \cdot \text{Im}[\tilde{n}]$ is the attenuation constant of the radiation in the material, d the sample thickness and λ the free-space radiation wavelength.

4. Experimental verification

In order to verify that the antennas indeed produce a large enhancement of the incoming THz radiation, we have assembled a simple THz setup, represented in Fig. 4(a).

To generate the THz radiation incident on the antenna structure, we employ a 2 step process:

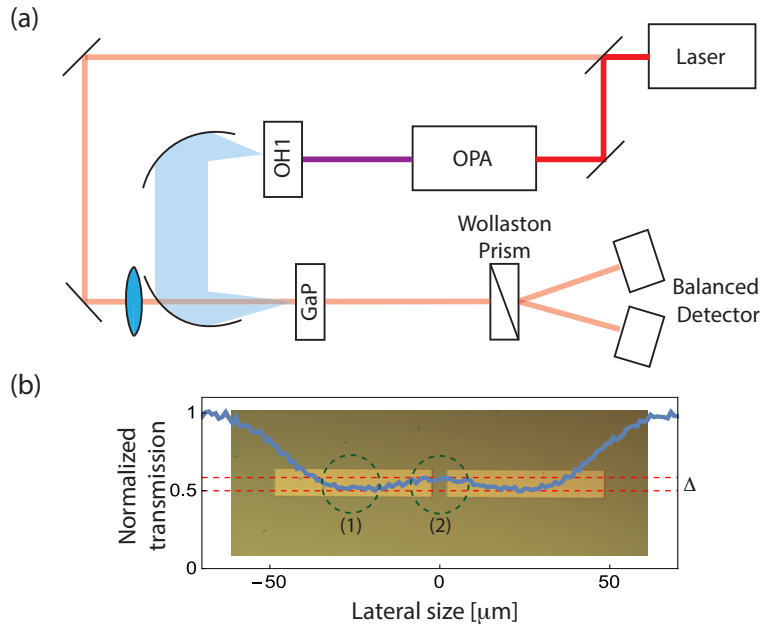


Fig. 4. (a) Schematic representation of the setup. (b) Optical image of a single antenna structure, overlaid by the normalized transmitted probe intensity measured scanning the antenna position. At the gap position an extra transmitted intensity Δ is measured. Positions (1) and (2): beam size and positions for the comparative measurements to extract the field enhancement.

first the output of a Ti:sapphire amplifier ($\lambda = 800$ nm, rep. rate $f = 1$ kHz, average pulse energy $E = 1.8$ mJ) is sent into an optical parametric amplifier (OPA) to generate longer wavelength light pulses ($\lambda_{OPA} = 1350$ nm, typical average pulse energy $E = 0.25$ - 0.3 mJ). In the second step we generate intense THz pump pulses via optical rectification of the infrared output of the OPA in an OH1 organic crystal. After filtering out the residual infrared beam, two off-axis parabolic mirror (PM) are used to collimate, and then focus the THz beam onto the sample. A small amount of the 800 nm ($< 1\%$) light is picked off before the OPA to be the probe beam. It is focused with a $f = 150$ mm-lens to a spot size of $d \approx 22$ μm FWHM at the sample position. The focal length of this lens is determined by the minimum distance available in our setup: we employ a collinear illumination between THz -pump and IR-probe, with the latter passing through a small (5 mm) aperture within the focusing PM, as depicted in Fig. 4(a). With this arrangement we can routinely achieve field strengths at focus exceeding 200 kV/cm (zero to peak) in an ambient atmosphere. The probe beam experiences a transformation of its polarization state from linear to elliptical by interacting with the GaP substrate due to the THz-induced electro-optic (EO) effect. A Wollaston prism together with a balanced amplifier photodetector collect the signal and its polarization changes as a function of the relative delay between pump and probe. A thorough description of an equivalent setup and signal interpretation is described in [40, 41].

The sample consists of a 100 μm -thick GaP substrate on top of which sets of isolated dipolar antenna with different sizes (arm length ranging between $L = 40$ μm to 65 μm , step size 5 μm) with a common gap of 4 μm and 10 μm width are deposited. In [19], Bagiante et al. describe the fabrication procedure. In brief, a thin layer Chromium (Cr), about 6 nm, was sputtered on the GaP and a double layer of resist (PMMA) was spinned on the Cr layer. The planar

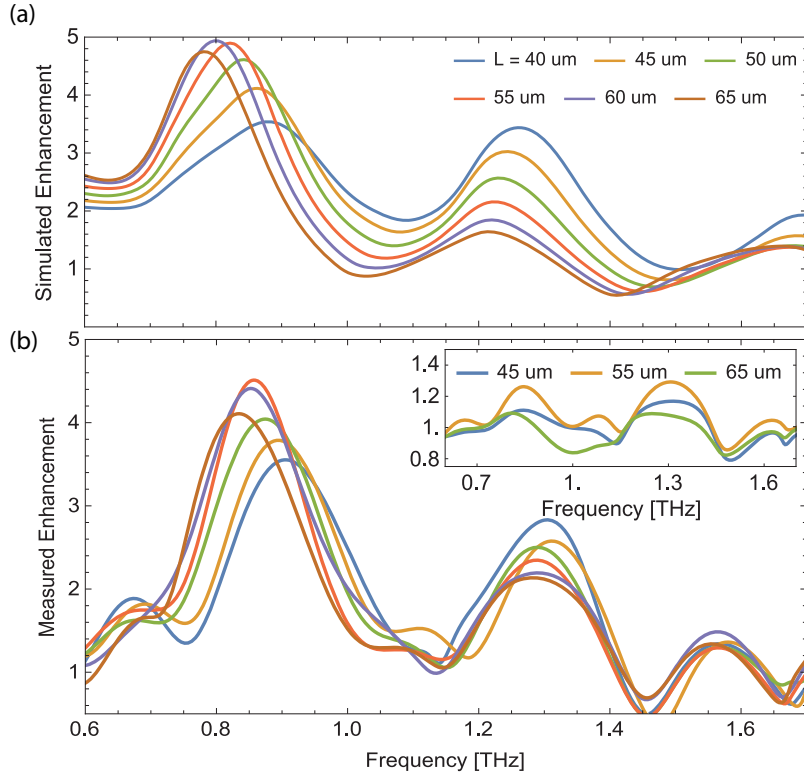


Fig. 5. Thickness integrated enhancement as a function of the antenna arm length L . (a) Simulated profiles, assuming plane wave illumination. (b) Extracted profiles from measurements. Inset: Extracted profiles from measurements in case of THz-polarization perpendicular to antennas axes.

structures were imprinted using electron-beam lithography. After the resist develop step, 1 nm of Cr and 100 nm of gold were deposited by an electron-beam evaporation. The Cr layer is essential to promote adhesion with the substrate. Finally, all excess metal was removed with lift-off technique and the remaining Cr on the GaP surface was removed by chloride reactive ion etching (RIE).

We image the antennas on the sample with a high-resolution camera equipped with a $20\times$ magnification objective. A typical antenna image is represented in Fig. 4(b). The antenna in the image is the $L = 45 \times 10 \mu\text{m}^2$ one. As described above, the probe beam size is limited to $d \approx 22 \mu\text{m}$ FWHM, thus a significant transmission is expected even from the sides of the antenna. The two dashed green circles in Fig. 4(b), represent the probe beam size (FWHM) compared with the antenna width. We have also collected the total intensity transmitted to the detection scheme as a function of the antenna position [Blue line overlay in Fig. 4(b)]. In position (1) [Fig. 4(b)] we have the minimum transmission, about 50% of the total radiation transmitted by the bare substrate (in very good agreement with the expected value of $T = 48.5\%$ considering the antenna and beam dimensions), whilst at the gap position (2) a small increment Δ is measurable.

The EO signal coming from the position (2) highlighted in Fig. 4 is the sum of the sides' [as at position (1)] plus gap's contributions. Therefore we can extrapolate the EO signal (EO_{gap}) coming from the gap by the following considerations. The light transmitted to the detector is:

$$I_{(1)} = I_0(T_{Au}f_{Au1} + T_{sub}f_{sub}), \quad (3)$$

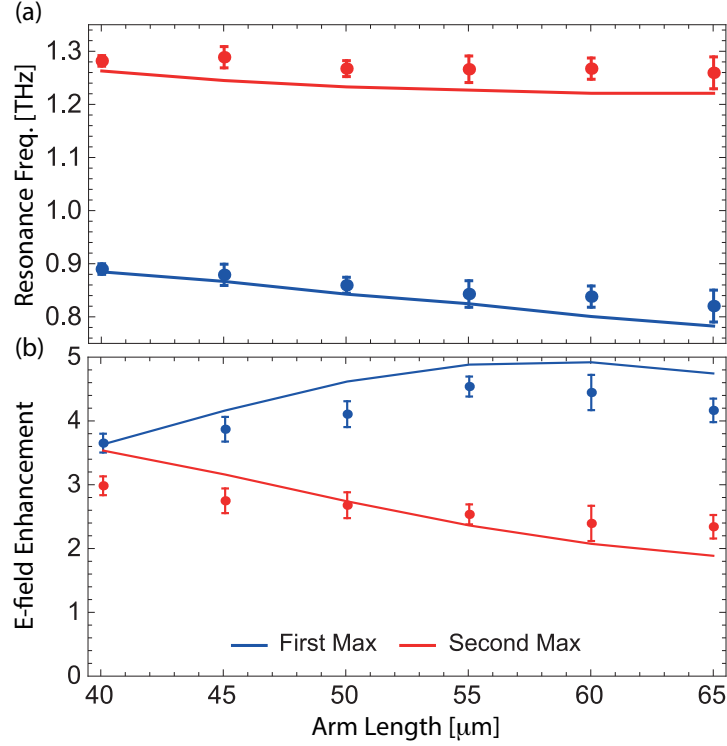


Fig. 6. Measured (a) Frequency and (b) Amplitude of the first two maxima of Fig. 5 as a function of the antenna arm length. Solid lines: corresponding simulated behavior.

$$I_{(2)} = I_0(f_{gap}T_{gap} + T_{Au}f_{Au2} + T_{sub}f_{sub}), \quad (4)$$

where I_0 is the impinging light intensity, $f_{gap(sub)}$ is the fraction of light impinging on the gap (directly on the substrate), $f_{Au1(2)}$ is the fraction of light impinging on the gold antenna at position $I(2)$, and $T_{Au(gap,sub)}$ are the amounts of light transmitted by the gold antenna, through the gap and at the air/substrate interface respectively. Since the antenna gap is considerably larger than the probe beam wavelength, diffraction effects from the gap itself can be neglected to leading order. Thus, in first approximation the transmission through the gap and the substrate is equivalent: $T_{gap} \approx T_{sub} = T$. We can also compute the transmission through the gold layer, as presented elsewhere [42, 43], and we find it negligible ($T_{Au} < 0.1\%$), therefore Eqs. (3) and (4) become:

$$I_{(1)} = I_0Tf_{sub}, \quad (5)$$

$$I_{(2)} = I_0T(f_{gap} + f_{sub}). \quad (6)$$

Since the signal measured due to the electro-optic effect ($EO_{(1)}$ and $EO_{(2)}$) is proportional to the probe intensity, the measured polarization rotation is a weighted average of contributions from different parts of the probed area:

$$EO_{(1)} = I_0Tf_{sub}EO_{sub}/I_0Tf_{sub} = EO_{sub}, \quad (7)$$

$$EO_{(2)} = (I_0Tf_{gap}EO_{gap} + I_0f_{sub}TEO_{sub})/(I_0Tf_{gap} + I_0Tf_{sub}). \quad (8)$$

From Eqs. (7) and (8), we can extract the EO signal contribution coming directly from the gap:

$$EO_{gap} = EO_{(2)} \left(1 + \frac{f_{sub}}{f_{gap}}\right) - \frac{f_{sub}}{f_{gap}} EO_{(1)} \quad (9)$$

where $EO_{gap,(1,2)}$ is the EO signal coming from the gap [area (1),(2) in Fig. 4]. By knowing the relative ratio of beam profile interacting with the gap and sample and performing two measurements, it is therefore possible to exactly reconstruct the EO sampling signal in the gap, thus the antenna enhancement effect. Moreover we must consider that the enhancements presented in Fig. 2 and Fig. 3 are simulated in the antenna plane. These NF effects exponentially decay with a length scale typically well within the first 10 μm .

Figure 5(a) shows the computed enhancement integrating the E-field amplitude throughout the full substrate thickness. We limit the frequency range between 0.6 - 1.7 THz, thus where the emission of OH1 is more efficient. It is apparent how the integration throughout the whole sample thickness is reducing the maximum expected enhancement to about 5.

Figure 5(b) shows the measured trends for the different antenna length in the frequency range under consideration. The traces compare reasonably well with the equivalent simulated ones. In particular, the position of the two peaks (scattered points), and its frequency dispersion is in good agreement with the simulated one (solid lines), as presented in Fig. 6. Also considering the maximum enhancement, measured data and simulated trends show compatible behavior. For example, for the lower frequency maximum, a field enhancement of about 5 times is expected for an antenna arm length of 60 μm , this being the largest effect. Accordingly, we measured the largest effect for the same antenna length. The maximum measured enhancement, integrated throughout the whole thickness is 4.6 times, which would correspond on a 28-fold increase at the sample surface. This translates to a THz field strength exceeding 5 MV/cm, for our simple experimental setup. Also the trend for the second maximum is well reproduced, although the measured length-dependence variation is smaller than the simulated one.

We have moreover investigated the enhancement in the case when the incoming THz polarization is set perpendicular to the main antenna axis. In the Inset of Fig. 5, a few of the resulting trends are presented. Within the experimental uncertainty no enhancement is observed, as expected [38].

5. Conclusion

Exploiting the resonant behavior of metallic structures, and their ability to confine and enhance the impinging radiation, we have designed isolated dipolar structure resonating at frequency of $f \approx 1$ THz. With a relatively simple experimental setup based on the electro-optical effect we can directly measure enhancement factors as high as 28 times of a freely propagating weak THz pulse (<200 kV/cm), resulting in a field strength exceeding 5 MV/cm at the sample surface. Moreover we find that the resulting near fields are strongly modulated in their frequency components. Based on computer simulations, we can explain this in terms of interference effects of the THz-radiation within the thin sample, which acts as a vertical cavity. Our investigations thus point out that in case of sample thinner than half the spatial pulse length, the sample thickness become an essential design parameter, which could be used to selectively amplify a specific frequency.

Acknowledgment

This work was supported by the NCCR Molecular Ultrafast Science and Technology (NCCR MUST), a research instrument of the Swiss National Science Foundation (SNSF).